Inorganic Chemistry

pubs.acs.org/IC Article

Polyoxometalate-Incorporated Framework as a Heterogeneous Catalyst for Selective Oxidation of C−H Bonds of Alkylbenzenes

Quanzhong Wang, Baijie Xu, Yingyue Wang, Hui Wang, Xin Hu, Pengtao Ma, Jingyang Niu,* and Jingping Wang*

Cite This: *Inorg. Chem.* 2021, 60, 7753−7761 Read Online

ACCESS | Metrics & More | Article Recommendations | Supporting Information

ABSTRACT: Developing new catalysts for highly efficient and selective oxidation of saturated C−H bonds is significant due to their thermodynamic strength. Via incorporation of $PW_{12}O_{40}^{3-}$, pyridine-2,5-dicarboxylic acids (pydc), and Fe(III) ions into one framework, a new polyoxometalate-based metal−organic framework, $[HFe_4O_2(H_2O)_4(pydc)_3PW_{12}O_{40}]\cdot 10.5H_2O$ (**FeW−PYDC**), was successfully prepared by a hydrothermal method. Interestingly, **FeW−PYDC** features a three-dimensional porous structure with $\{Fe_4O_2\}$ interconnecting with $PW_{12}O_{40}^{3-}$ units. **FeW−PYDC** displayed excellent performance in the selective oxidation of C−H bonds of alkylbenzenes with high conversion (95.7%) and selectivity (96.6%). As an effective heterogeneous catalyst, **FeW−PYDC** demonstrates good reusability and structural stability.

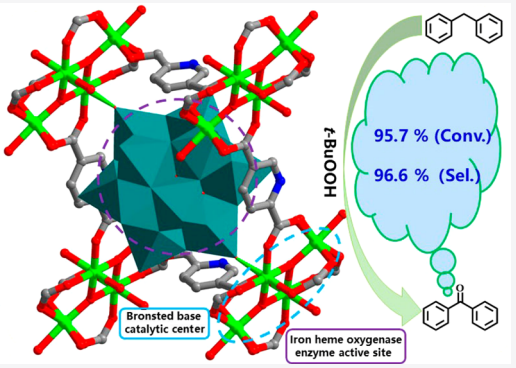

Downloaded via TSINGHUA UNIV on August 10, 2021 at 17:40:27 (UTC).
See https://pubs.acs.org/sharingguidelines for options on how to legitimately share published articles.

1. INTRODUCTION

Today, C−H oxidation is a primary and key technology for the preparation of many different organic compounds.[1,2] However, because saturated C−H bonds are thermodynamically strong and dynamically inert, the selective oxidation of elementary C−H bonds is a great challenge in both industrial and academic aspects.[3−5] It is worth noting that the selective oxidation of alkylbenzenes has created widespread interest in many fields, including but not limited to the petrochemical industry, the pharmaceutical industry, the production of functional materials, etc.[6−8] To the best of our knowledge, some Pd^{-}- or Ru^{-}-containing complexes[9−11] and numerous organic molecules[12−16] have been reported as effective catalysts for achieving C−H oxidation. However, the noble metal-based homogeneous catalysts are normally neither affordable nor recyclable; thus, they do not meet the economic and environmental standards.[17,18] Hence, the exploration of green and recyclable catalysts capable of working in a heterogeneous manner is of considerable interest.

Fe(III)-incorporated catalysts have been well developed because they not only can oxidize the C−H bonds but also can result in high selectivity control. In particular, chemists employ a number of heme[19] and nonheme[20] iron enzymes, for the purpose of carrying out such transformations.[21,22] For example, the cytochrome P450 is capable of performing hydroxylation of aliphatic C−H groups with dioxygen with high regio- and stereoselectivity.[23] The active oxidant in Rieske dioxygenase also can be generated by the peroxide shunt pathway[24] and can mediate a variety of oxidations. Iron heme oxygenase (IHO) has attracted the attention of chemists because of its unique spectral properties in efficiently catalyzing a wide range of difficult biotransformations.[25] The iron−oxo unit is involved in many catalytic cycles of nonheme iron enzymes, and analogous biomimetic oxidants can perform hydroxylation and oxygen atom transfer reactions. Inspired by such intriguing processes, many chemists have been devoted to the emulation hemoglobin model reaction cascades by developing auto-tandem catalytic reactions. The active sites in all of these systems likely contain μ-O, μ-H, or μ-COOH double iron cores, and Fe^{3+} ions have been thought to serve as the major active intermediate in the majority of biological oxidation events. The interaction of the Fe^{3+} with TBHP (*t*-BuOOH) results in the Fe^{3+}−OOBu-t species.[26−29] With the heterolytic cleavage of the O−O bond, Fe^{V}−O intermediate oxidizing species and *t*-BuO·radical species are generated.[19,24] These changes would obviously enhance the oxidative reactivity of the central metal ions. This process can promote the formation of oxidant free radicals during catalysis.[30−33]

Polyoxometalates (POMs), along with their excellent thermal and oxidative stability and high efficiency under homogeneous conditions, have attracted a great deal of attention as highly selective oxidation catalysts.[34−37] In particular, iron-substituted polyoxometalate (Fe-POM)

Received: January 15, 2021
Published: May 21, 2021

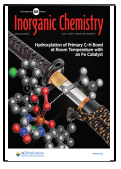

ACS Publications © 2021 American Chemical Society

https://doi.org/10.1021/acs.inorgchem.1c00135
Inorg. Chem. 2021, 60, 7753−7761

showed better performance in the monooxygenation of organic compounds than saturated Keggin-type and Dawson-type POMs, due to the tuning of the electronic structure and high stability of the redox states.[38] In 2005, Neumann's group reported an Fe-substituted POM (POM-FeO_4^-), which is a powerful oxidant with C−H hydroxylation and C−C epoxidation ability.[39] In addition, the incorporation of POMs and Fe^{3+} ions into metal organic frameworks (MOFs) can overcome poor thermal stability, increase the specific surface area, and promote the synergic effects between multifunctional catalytic sites of Fe^{3+} and POM units, thus expanding its application range in various selective oxidation catalytic systems.[40−42] For example, in 2020, Han's group reported a new FeW-DPNDI incorporating the trimer of the Fe-substituted Dawson derivative, which shows high performance in the photocatalytic toluene oxidation under mild conditions.[43] Therefore, the design and development of new nonheme-like diiron site-incorporated POM-based catalysts will be an effective approach to achieving the selective oxidation of C−H bonds.[44]

By incorporating Keggin-type $PW_{12}O_{40}^{3-}$ anions, Fe^{3+} ions, and pyridine-2,5-dicarboxylic acids (pydc) together, we successfully obtained a new Fe-incorporated POMOF, $[HFe_4O_2(H_2O)_4(pydc)_3(PW_{12}O_{40})]\cdot 10.5H_2O$ (**FeW−PYDC**). **FeW−PYDC** features a three-dimensional (3D) porous structure in which the nonheme-like $\{Fe_4O_2\}$ interconnects with $PW_{12}O_{40}^{3-}$ units. Inspiringly, the Fe^{3+} site in the $\{Fe_4O_2\}$ cluster is effective in catalyzing the C−H bond oxidation reactions through the synergy of the catalytic active sites. The TBHP (*t*-BuOOH) interacts with Fe^{3+} to form the Fe^{3+}−OOBu-*t* species.[26−29] Heterolytic cleavage of the O−O bond in Fe^{3+}−OOBu-*t* species forms *t*-BuO• and •OH radicals and further oxidizes the substrates into ketones.[45−47] The unique redox properties of $\{Fe_4O_2\}$ with its oxo−iron unit provide sufficient driving force in transforming catalytic precursors into active intermediates and further trigger the oxidation reaction (Scheme 1).[48] The introduction of pydc provides amphiphilic channels for accommodating both hydrophilic TBHP and hydrophobic substrates.[49−51] Concurrently, the pydc ligand helps to enhance the stability of **FeW−PYDC** because of its high stability and oxidation inertness.

Scheme 1. Design a Catalyst Using the Synergistic Effect between the Cation in the Polyanion Components and $\{Fe_4O_2\}$ Clusters

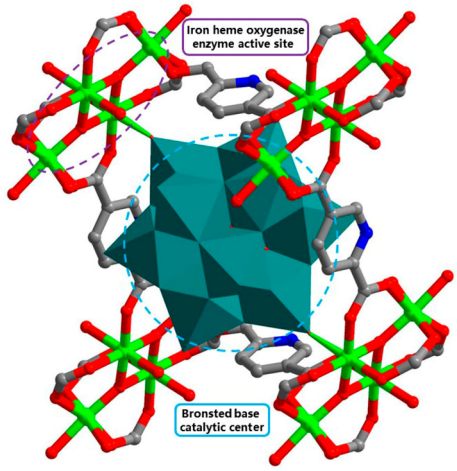

2. RESULTS AND DISCUSSION

2.1. Crystal Structure. Single-crystal X-ray diffraction structural analysis reveals that **FeW−PYDC** crystallizes in space group *P*1̄. The crystal structure consists of an $\{Fe_4O_2\}$ cluster, three pydc ligands, a Keggin-type $PW_{12}O_{40}^{3-}$ as the basic building block, four coordination water molecules, and some extra noncoordinated lattice water molecules. There are two crystallographically independent Fe^{3+} ions. Each Fe^{3+} adopts a hexacoordinated environment in a distorted octahedral coordination geometry. Fe1 bonds to three oxygen atoms from three different pydc ligands, two bridging oxygen atoms, and one terminal oxygen atom originating from $PW_{12}O_{40}^{3-}$ (Figure S3), while Fe2 is coordinated with three oxygen atoms from three different pydc ligands, two oxygen atoms originating from water molecules, and one bridging oxygen atom (Figure S4). The Fe−O bond lengths are in the range of 1.830(11)−2.080(2) Å, and the O−Fe−O bond angles are in the range of 83.1(7)−176.4(8) ° (Table S1). The coordinated water molecules around the Fe^{3+} center are conveniently removable, enabling the Fe^{3+} center to interact with oxygen atoms of TBHP as an active Lewis acid catalyst. Both Fe1 and Fe2 atoms are interconnected with two μ_3-oxo atoms, thus forming a diamond-like $\{Fe_4O_2\}$ cluster (Figures S1 and S5). $\{Fe_4O_2\}$ clusters are further interlinked by dicarboxylic ligands; in particular, each $\{Fe_4O_2\}$ cluster connects with six dicarboxylic ligands (Figure 1) in a different orientation, therefore resulting in a 3D infinitely extended framework. $\{Fe_4O_2\}$ clusters can advantageously provide abundant metal active sites, thereby enhancing the catalytic efficiency of the **FeW−PYDC** catalyst.

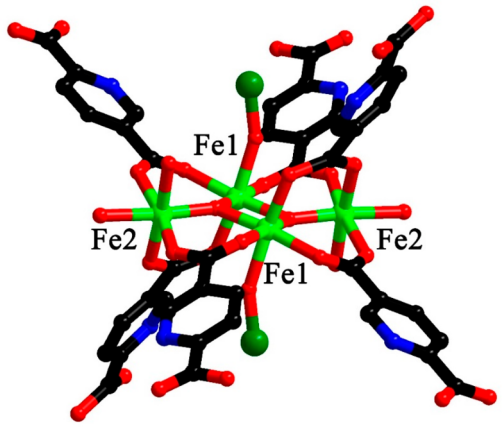

Figure 1. Coordination mode of $\{Fe_4O_2\}$. Color code: O, red; C, black; N, blue; Fe, green; W, dark green.

In the Keggin structure, eight O atoms around the P atom for PO_4 were observed, in which all of these peripheral O atoms are all at half-occupancy. Additionally, one pyridine-2,5-dicarboxylate ligand also has a high degree of disorder, and it can be viewed as the ligand skeleton flipping along the C11−C11A (symmetric code: A = −1 − *X*, 1 − *Y*, −*Z*) axis. The $PW_{12}O_{40}^{3-}$ scaffold links two $\{Fe_4O_2\}$ clusters via its two terminal oxygen atoms from two opposite $\{W_3O_{13}\}$ fragments (Figure 2). If we ignore POM for the sake of simplicity, the $\{Fe_4O_2\}$ cluster and six affiliated ligands are likely forming a

https://doi.org/10.1021/acs.inorgchem.1c00135
Inorg. Chem. 2021, 60, 7753−7761

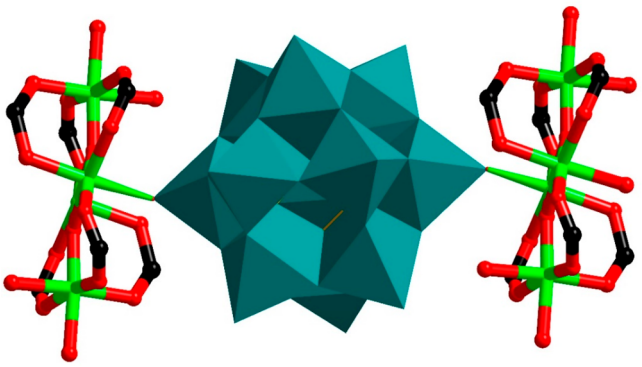

Figure 2. Coordination mode of $PW_{12}O_{40}^{3-}$.

crown-shaped structure (Figure S7). Likewise, in the absence of ligands, two POMs form a dumbbell-like shape bridged by two symmetric Fe1 ions (Figure S8). Meanwhile, due to the abundant surface negative charges, $PW_{12}O_{40}^{3-}$ is beneficial for the combination with H^+, thus displaying a strong Brønsted base catalytic performance. Bond valence sum (BVS) calculations show that the P center and W atoms are all conventionally in +5 and +6 oxidation states (Table S2), while Fe atoms are all in +3, which is strongly evidenced by X-ray photoelectron spectroscopy (XPS) (Table S3 and Figure 6a).[52]

In this coordination mode, the host framework contains two kinds of metal−organic macrocycles named macrocycle A and macrocycle B. Macrocycle A is composed of four pydc ligands commutatively interconnected with three neighboring Fe atoms to form $[Fe_{12}(pydc)_4]$ with dimensions of ∼19.67 Å × ∼8.01 Å (Figure S5a). In addition, a one-dimensional (1D) loop-containing chain consists of macrocycle A by edge sharing fixed by an adjacent neighbor (Figure 3a). In addition, a novel

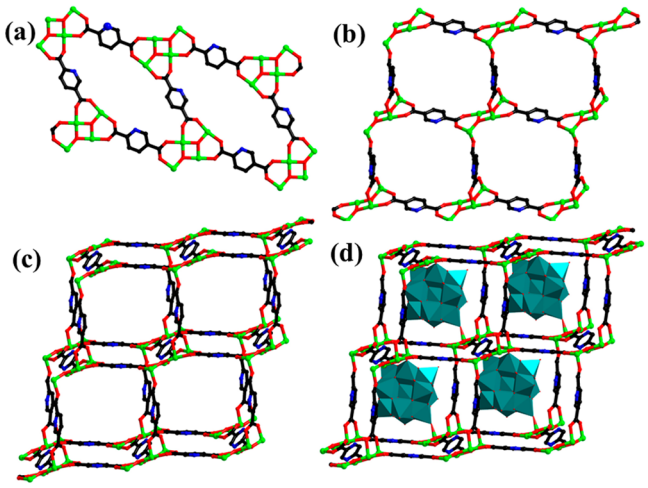

Figure 3. (a) 1D loop-containing chain in a 2D host double-layer framework. (b) 2D layer based on edge-sharing large rings. (c) 2D host double-layer framework. (d) 3D framework of **FeW−PYDC**.

$[Fe_{12}(pydc)_4]$ macrocycle B is also constructed by four pydc ligands to link adjacent Fe atoms, and the window has dimensions of ∼13.12 Å × ∼12.64 Å (Figure S5b). Unlike macrocycle A, a two-dimensional (2D) layer is formed from each macrocycle B linked with three other neighbors (Figure 3b). Two parallel 2D layers and the 1D loop containing chains via O−Fe1−O30 and O−Fe2−O linkages are bridged in a vertical direction forming a 2D double-AB_2 layer (Figure 3c). After being introduced into the pore, the guest containing the catalytic active site can be easily used in the catalytic reaction. More specifically, the PW_{12} (∼10.39 Å × ∼10.48 Å) is smaller than the AB2 layer structure (∼11.12 Å × ∼12.85 Å). As a consequence, the $PW_{12}O_{40}^{3-}$ anion can be successfully trapped in the 2D double-AB_2 layer and stabilized by Fe−O bonds (Figure 3d). In addition, the introduction of POMs joins two identical double-layer networks to give a complicated 3D POMOF structure through the Fe−O linker, which helps to stabilize the entire framework to some extent. As shown in Figure S9, **FeW−PYDC** was simplified as a 3D framework with a new topology of $\{4^2.7^3.9\}\{4^2.7^4\}\{4^2.8^2.9.10\}\{4^3\}_2\{4^4.6^2\}_2\{4^5.6^3.7^4.8^2.9\}_2$. The total solvent-accessible volume accounts for approximately 23.2% of the whole crystal volume as estimated by PLATON.[53] The N_2 adsorption−desorption isotherms were measured at 77 K, and the corresponding pore diameter distribution of the **FeW−PYDC** catalyst is presented in Figure S10. The Barrett−Joyner−Halenda (BJH) plot of **FeW−PYDC** reveals a wider pore distribution with two types of mesopores, with the smaller mesopores centered at ∼6.8 nm and the larger mesopores centered at ∼12.8 nm. The presence of large mesopores in **FeW−PYDC** is advantageous to both hydrophilic TBHP (Figure S11a) and hydrophobic (Figure S11b) substrates entering the pores and making contact with active centers inside the mesopores and facilitates the transmission of the catalytic reaction substrates and products.

2.2. Characterizations of FeW−PYDC. The good match between the experimental powder X-ray diffraction (PXRD) and the simulated pattern confirmed the good phase purity of **FeW−PYDC** (Figure 4a and Figure S12). Importantly, **FeW−PYDC** exhibits excellent chemical stability and retains good crystallinity after several months. Even after being refluxed in organic solvents (acetonitrile, cyclohexane, and benzonitrile), it still retains its structural integrity, as verified by the infrared (IR) spectrum (Figure 4c) and the PXRD pattern (Figure 4b

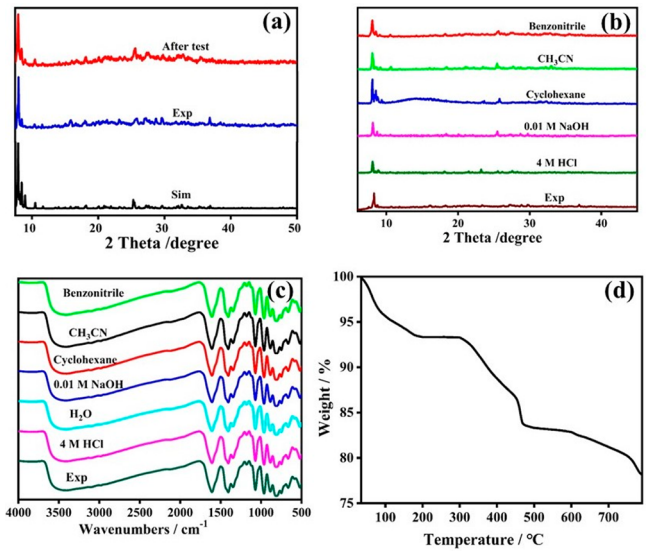

Figure 4. (a) PXRD patterns of **FeW−PYDC** before and after catalysis. (b) PXRD patterns of **FeW−PYDC** in different solutions compared with experimental curves. (c) Infrared spectrum of **FeW−PYDC** in different solutions compared with experimental curves. (d) TG curve of **FeW−PYDC** between 30 and 800 °C.

https://doi.org/10.1021/acs.inorgchem.1c00135
Inorg. Chem. 2021, 60, 7753−7761

and Figure S13). It also displayed high acid and alkali resistance in 4 M HCl and 0.01 M NaOH, respectively, for 48 h. As shown in Figure 4d, thermogravimetric analysis (TGA) of **FeW−PYDC** exhibits three steps of weight loss. The first weight loss of 6.57% (calcd 6.59%) between 80 and 300 °C corresponds to the loss of 14.5 water molecules and indicates that **FeW−PYDC** has fine thermodynamic stability. A second weight loss of 10.5 wt % occurred between 300 and 800 °C, where the skeleton begins to collapse, and corresponds to the removal of the pydc ligand. Finally, the third weight loss starts at a higher temperature (>600 °C) with the local collapse of $PW_{12}O_{40}^{3-}$ clusters. **FeW−PYDC** exhibits high chemical and thermal stability and meets most of the prerequisites as an ideal platform for heterogeneous catalysis in oxidation of diphenylmethane to benzophenone.

2.3. Catalytic Oxidation of Alkylbenzenes. The catalysis oxidation of C−H bonds was initially examined using diphenylmethane as the model substrate and TBHP as the oxidant, along with **FeW−PYDC** in a heterogeneous reaction. To optimize the experimental conditions, catalyst dosages, TBHP amounts, temperature, and solvent were extensively investigated. First, the diphenylmethane oxidation was carried out in benzonitrile at 70 °C for 24 h using TBHP as the oxidant with different dosages of catalyst **FeW−PYDC** (Figure S14). As shown in Figure 5a, the increase in the

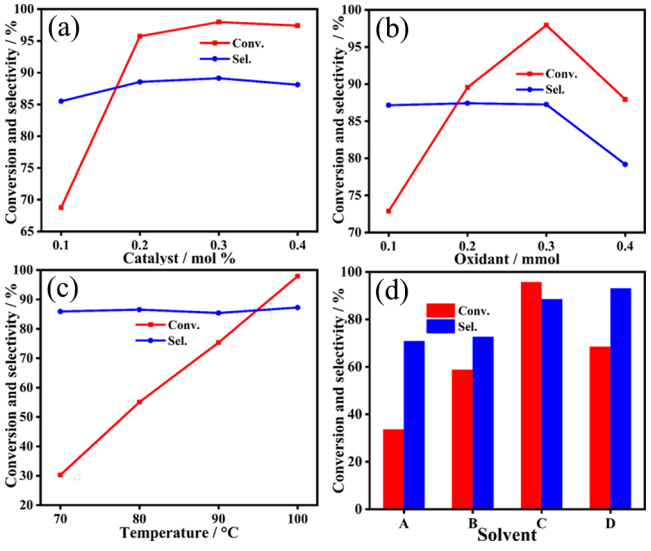

Figure 5. Effect on the conversion and selectivity of the catalytic oxidation of diphenylmethane of (a) different quantities of **FeW−PYDC**, (b) different quantities of TBHP, (c) different temperatures, and (d) different solvents (A, cyclohexane; B, acetonitrile; C, benzonitrile; D, *n*-hexane). Other reaction conditions: diphenylmethane (1 mmol), solvent (0.5 mL), and 24 h.

catalyst dosage greatly accelerated the oxidation reaction. When the dosage increased from 0.1 to 0.3 mol %, the catalytic rate was conspicuously improved, and the conversion and selectivity show an escalating trend. Nevertheless, as the amount of catalyst increased to 0.4 mol %, the conversion was not obviously improved. Therefore, the optimum dosage of the catalyst is identified as 0.3 mol %. Second, the TBHP amount also affects the catalytic efficiency. As illustrated in Figure 5b, with an increase in the TBHP amounts from 1.0 to 4.0 mmol, the oxidation efficiency of diphenylmethane first increased until the amount reached 3.0 mmol and then decreased. With the increase in TBHP amounts, more *t*-BuO• and •OH radical species were generated to oxidize diphenylmethane, but the excess TBHP was also regarded as a scavenger of the *t*-BuO• radical species. Therefore, an optimal TBHP amount of 3.0 mmol is available for the best oxidation efficiency of diphenylmethane.

Then, the reaction temperature was also tested from 70 to 100 °C, and a roughly linear relationship between the target product and the reaction temperature was achieved; when the temperature was increased to 100 °C, the oxidation exhibited high conversion (95.7%) and selectivity (87.3%) (Figure 5c). Moreover, different solvents (acetonitrile, cyclohexane, benzonitrile, and *n*-hexane) were also studied; by comparison, benzonitrile is the most compatible solvent for obtaining much higher conversion and selectivity simultaneously (Figure 5d). On the basis of the results presented above, we established the optimal reaction conditions; namely, 0.3 mol % catalyst, 3 mmol of TBHP, reaction temperature of 100 °C, 24 h, and a benzonitrile solvent are used for the best oxidation of diphenylmethane, showing high conversion (95.7%) and selectivity (96.6%). **Caution!** Benzonitrile is a highly toxic reactant. Thus, suitable care, precautions, and protection for handling of such substances were employed.

Several control experiments were conducted in the selective oxidation of diphenylmethane to benzophenone. The blank experiment gave a conversion of only 20.6% (Table 1, entry 1).

Table 1. Catalytic Oxidation of Diphenylmethane Using Different Catalysts[a]

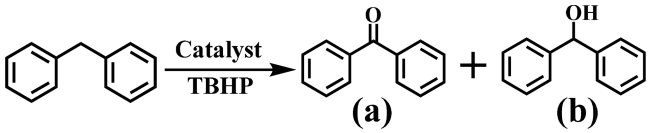

entry	catalyst	reaction system	conversion[b] (%)	selectivity (%)
1	–	–	20.6	79.3
2	PW_{12}	homogeneous	48.5	66.9
3	$FeCl_3$	homogeneous	66.5	83.6
4	pydc	heterogeneous	21.3	80.0
5	pydc/$FeCl_3$/PW_{12}	heterogeneous	55.5	69.3
6	**FeW−PYDC**	heterogeneous	95.7	96.6
7	**FeW−PYDC**/IPA[c]	heterogeneous	13.16	46

[a]Reaction conditions: diphenylmethane (1 mmol), TBHP (3 mmol), catalyst (0.3 mol %), benzonitrile (0.5 mL), 100 °C, and 24 h. [b]GC conversion and selectivity for target product benzophenone measured on the basis of naphthylene as the internal standard. All of the products were identified by GC−MS and GC spectra. [c]Isopropanol as the •OH scavenger.

The raw materials used to synthesize **FeW−PYDC**, such as $FeCl_3$, $PW_{12}O_{40}^{3-}$, and pydc, were also introduced into the catalytic reaction mixtures for a control study. The use of $PW_{12}O_{40}^{3-}$ as a homogeneous catalyst could give a medium conversion (48.5%) and selectivity (66.9%). $PW_{12}O_{40}^{3-}$ can activate the corresponding W═O_t to generate an active peroxide tungstate intermediate with TBHP, thereby ensuring the smooth progress of the reaction.[34]

Using isopropanol (IPA) as a hydroxyl radical (•OH) scavenger, the product yield decreased significantly to 13.2% (Table 1, entry 7).[54] Thus, we surmised that •OH generated from TBHP as a necessary product in the selective oxidation of

https://doi.org/10.1021/acs.inorgchem.1c00135
Inorg. Chem. 2021, 60, 7753−7761

Table 2. Catalytic Oxidation of Different Organic Substrates[a]

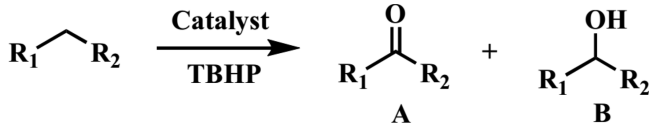

Entry	Substrate	Conv[b]. / %	Product A (%)	Product B (%)
1	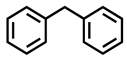	95.7	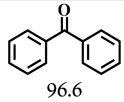 96.6	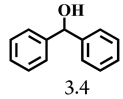 3.4
2	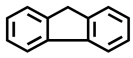	66.3	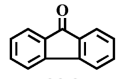 90.8	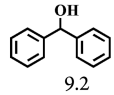 9.2
3	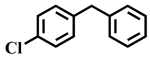	93.1	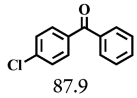 87.9	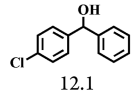 12.1
4		92.7	 100	—
5	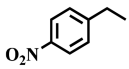	95.5	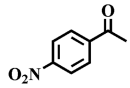 94.1	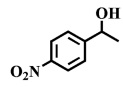 5.9
6	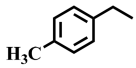	90.3	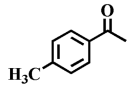 87.6	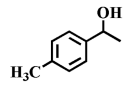 12.4

[a]Reaction conditions: substrates (1 mmol), TBHP (3 mmol), catalyst (0.3 mol %), 100 °C, and benzonitrile (0.5 mL).[b] [b]GC conversion and selectivity for target products measured on the basis of naphthylene as the internal standard. All of the products were identified by GC−MS and GC spectra.

Table 3. Summary of the Catalytic Diphenylmethane Oxidation over Many Catalysts

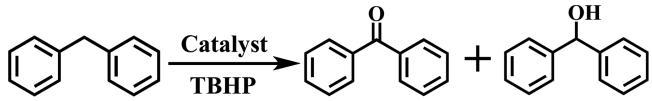

catalyst	substrate (mmol)	solvent	conversion[a] (%)	selectivity (%)	ref
HKUST-1@Fe_3O_4	0.25	benzonitrile	94.7	95.2	55
$PNb_{12}O_{40}(VO)_2$	0.04	benzonitrile	93.4	91.3	56
$\{[CdMn^{III}(DMF)_6TPyP](PW_{12}O_{40})\}\cdot 5H_2O$	0.1	H_2O	92.7	100	57
FeW−PYDC	1	benzonitrile	95.7	96.6	this work

[a]GC conversion and selectivity for target product benzophenone measured on the basis of naphthylene as the internal standard. All of the products were identified by GC−MS and GC spectra.

C−H bonds of alkylbenzenes played a particular role in the reaction process. When $FeCl_3$ was introduced as a catalyst, the reaction gave a better conversion (66.5%) and selectivity (83.6%) versus those with $PW_{12}O_{40}^{3-}$ (Table 1, entry 3), which indicates that the Fe^{III} ion plays a very important role in improving the catalytic activity. The unique redox properties of Fe with its oxo−iron unit provide sufficient driving forces that ensure the transformation of catalytic precursors to active intermediates, which activates the O−O bond of TBHP (*t*-BuOOH) and forms *t*-BuO• and •OH radical species and, subsequently, further oxidizes the substrates and generates the corresponding ketone compounds.[45,51] In addition, the physical mixture of $FeCl_3$, $PW_{12}O_{40}^{3-}$, and pydc under the same reaction conditions led to a comparable conversion (55.5%) and reaction selectivity (69.3%) (Table 1, entry 5).

The substrate scope has been expanded by employing a variety of benzylic C−H compounds under the optimized reaction conditions. The corresponding ketones were successfully synthesized with great conversion (66.3−95.7%) and selectivity (87.6−96.6%) when using **FeW−PYDC** as the catalyst (Table 2). These preliminary results prove that **FeW−PYDC** serves as a highly efficient and selective catalyst to facilitate the oxidation of various benzylic C−H bonds. Indeed, **FeW−PYDC** outperforms many other heterogeneous catalysts reported to date, such as nanocomposite HKUST-1@Fe_3O_4,[55] and $\{[CdMn^{III}(DMF)_6TPyP](PW_{12}O_{40})\}\cdot 5H_2O$,[57] $PNb_{12}O_{40}(VO)_2$,[56] and **FeW−PYDC** gave higher conversions, which might be ascribed to the unique redox properties of $\{Fe_4O_2\}$ with its oxo−iron unit (Table 3 and Table S4).

https://doi.org/10.1021/acs.inorgchem.1c00135
Inorg. Chem. 2021, 60, 7753−7761

2.4. Recyclability and Stability. To verify the heterogeneity and recyclability of the catalyst, the leaching experiment was carried out. The removal of **FeW−PYDC** (by filtration) immediately deactivated the catalytic process as supported by Figure S15, where the filtrate afforded nearly no additional products even after stirring for an additional 12 h. These observations strongly suggest that **FeW−PYDC** is a true heterogeneous catalyst. Furthermore, the **FeW−PYDC** catalyst could be retrieved from the reaction system by simple filtration and reused for at least three reaction cycles with moderate activity loss: the reaction yield decreases from 95.7% to 83.6% along with a slight decrease in selectivity from 96.6% to 91.2% (Figure S16). The PXRD and IR patterns of recycled **FeW−PYDC** match well with those of fresh samples, indicating its strong structural stability. The XPS results provide additional evidence by verifying the identical valence states of Fe1 and Fe2 in **FeW−PYDC** pre- and postcatalysis (Figure 6b).[58,59] In addition, no W and Fe elements were discovered in the recycled filtrate by ICP, which further proves the stability of **FeW−PYDC** during the successive catalytic reactions.

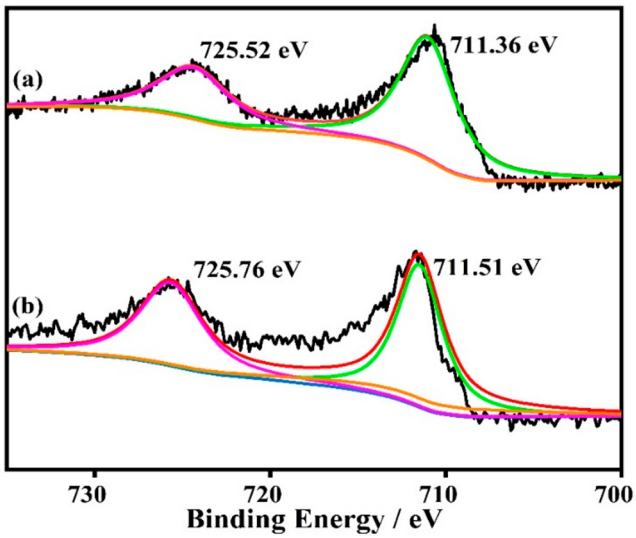

Figure 6. XPS Fe 2p spectra for (a) fresh **FeW−PYDC** and (b) recovered **FeW−PYDC**.

2.5. Kinetic Study. To further research the reaction dynamics, the reaction mixture was collected at regular intervals (4 h) using GC to monitor the reaction progress. As illustrated in Figure 7, both reaction conversion and $\ln(C_t/C_0)$ are plotted versus the reaction time at the optimal temperature of 100 °C, where C_0 represents the concentrations at the beginning of reaction and C_t represents the concentration at each time point, $\ln(C_t/C_0)$ represents a strong linear regression versus reaction time (R^2 = 0.99964), and the value of reaction rate constant k was calculated to be 0.13537 h^{-1}. The same linear tests were performed for the catalytic reaction data at other temperatures (90 and 110 °C), and the results showed that the catalytic experiments were in accord with the kinetic characteristics of the first-order reaction within the temperature range tested (Figure S19a,c); the corresponding rate constants k were 0.10368 and 0.15154 h^{-1}, respectively (Figure S19e). As shown in Figure S19d, the conversion of the product displayed a gradual upward trend at different temperatures within the 24 h detection time range when **FeW−PYDC** was used in the system. In addition, increasing the reaction temperature from 90 to 110 °C leads to an increase in the conversion from 90.7% to 96.5%, indicating that the activity of this catalytic reaction was significantly affected by the temperature. On this basis, the activation energy (E_a) of the oxidation of diphenylmethane catalyzed by **FeW−PYDC** under optimal conditions was calculated according to the Arrhenius law to be 27.3 kJ mol^{-1} (Figure S19f). In addition, the activation enthalpy ($\Delta H^{\ddagger}$) was determined to be 23.8 kJ mol^{-1}, the activation entropy ($\Delta S^{\ddagger}$) −236.6 J mol^{-1} K^{-1}, and the Gibbs energy ($\Delta G^{\ddagger}$) 104.3 kJ mol^{-1}. The negative entropy value suggested an associative process involved in the rate-limiting step.[60]

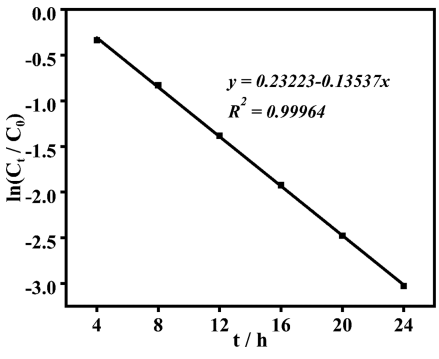

Figure 7. Kinetic study of oxidation of diphenylmethane catalyzed by **FeW−PYDC**.

3. CONCLUSION

In conclusion, a new iron-containing 3D framework **FeW−PYDC** was successfully synthesized by a hydrothermal method and well characterized. Structural analyses indicate that the **FeW−PYDC** framework is composed of Fe^{3+} and polyanion components interconnected by pydc ligands. Notably, in this metal−organic framework, $\{Fe_4O_2\}$ is formed as the fundamental nodes and all of the Fe^{3+} ions adopt a hexacoordinated environment. Herein, **FeW−PYDC** has been demonstrated to be an effective heterogeneous catalyst for oxidizing diphenylmethane to benzophenone in a pseudo-first-order kinetic manner. Specifically, **FeW−PYDC** has exhibited high reaction conversion (95.7%) and selectivity (96.6%) under the optimized reaction condition, outperforming many other heterogeneous catalysts. A mechanistic study showed that **FeW−PYDC** may facilitate the formation of *t*-BuO• and •OH radical species and, subsequently, oxidize the substrates to ketones. Furthermore, **FeW−PYDC** represents excellent recyclability and stability, assisted by its heterogeneous nature. More importantly, we believe the successes of **FeW−PYDC** as a heterogeneous catalyst activating stable C−H bonds should lead to a new approach in designing novel POM-based catalysts for many other applications.

4. EXPERIMENTAL SECTION

4.1. Materials and Methods. All chemicals and reagents used in this study were reagent grade and used without further purification. $H_3PW_{12}O_{40}\cdot 15H_2O$ was synthesized accroding to the literature.[61] The elemental analyses (EA) of C, H, and N were performed on a Vario EL III elemental analyzer. Inductively coupled plasma optical emission spectroscopy (ICP) of Fe, P, and W was performed on a Jarrel-Ash model J-A1100 spectrometer. IR spectra were collected from the powder sample with KBr pellets as a base on a JASCO FT/IR-430 spectrometer. Thermogravimetric analysis was performed on a

https://doi.org/10.1021/acs.inorgchem.1c00135
Inorg. Chem. 2021, 60, 7753−7761

Table 4. Crystal Data and Structural Refinement of FeW−PYDC

empirical formula	$C_{21}Fe_4N_3O_{59}PW_{12}$
formula weight	3698.81
crystal system	triclinic
space group	$P\bar{1}$
a (Å)	12.8533(5)
b (Å)	13.1878(6)
c (Å)	13.3075(5)
α (deg)	115.3610(10)
β (deg)	108.8460(10)
γ (deg)	98.9700(10)
volume (Å^3)	1811.24(13)
Z	1
ρ_{calc} (g/cm^3)	3.391
μ (mm^{-1})	19.864
F(000)	1626.0
crystal size (mm^3)	0.16 × 0.14 × 0.12
2θ range for data collection (deg)	5.376−50.198
index ranges	$-15 \le h \le 15$, $-15 \le k \le 15$, $-15 \le l \le 14$
no. of reflections collected	21824
no. of independent reflections	6419 (R_{int} = 0.0518; R_σ = 0.0516)
data/restraints/parameters	6419/211/460
goodness of fit on F^2	1.036
R_1,[a] wR_2[b] [$I \ge 2\sigma(I)$]	R_1 = 0.0763, wR_2 = 0.1543
R_1,[a] wR_2[b] (all data)	R_1 = 0.0985, wR_2 = 0.1673

[a] $R_1 = \sum||F_o| - |F_c||/\sum|F_o|$. [b] $wR_2 = [\sum w(F_o^2 - F_c^2)^2/\sum w(F_o^2)^2]^{1/2}$; $w = 1/[\sigma^2(F_o^2) + (xP)^2 + yP]$, where $P = (F_o^2 + 2F_c^2)/3$, where x = 0.0396 and y = 112.8222 for **FeW−PYDC**.

Mettler-Toledo TGA/SDTA 851e instrument heated from 25 to 800 °C at a heating rate of 10 °C min^{-1}, under a dynamic nitrogen atmosphere. The powder X-ray diffraction (PXRD) patterns were recorded on a Bruker D8 Advance instrument with Cu Kα radiation (λ = 1.5418 Å). X-ray photoelectron spectroscopy (XPS) was performed with an Axis Ultra X-ray photoelectron spectrometer. GC analyses were performed on a Bruker 450-GC instrument with a flame ionization detector equipped with a 30 cm column (GsBP-5, 0.25 mm internal diameter and 0.25 μm film thickness) with nitrogen as the carrier gas.

4.2. Preparation of FeW−PYDC. **FeW−PYDC** was prepared under hydrothermal conditions by the self-assembly approach. $H_3PW_{12}O_{40}\cdot 15H_2O$ (0.10 mmol, 300 mg), $FeCl_3\cdot 9H_2O$ (2 mmol, 540 mg), and pydc (1 mmol, 167 mg) were dissolved in 10 mL of distilled water at room temperature. The resulting suspension was stirred for 60 min, sealed in a 30 mL Teflon-lined reactor, and heated at 160 °C for 5 days. After slowly cooling to room temperature at a rate of 10 °C h^{-1}, yellow block crystals of **FeW−PYDC** were isolated, collected by being washed three times with distilled water, and then air-dried to give a yield of 70% (based on W). Elemental analysis (%) calcd for $C_{21}Fe_4N_3O_{59}PW_{12}$ (M_r = 3698.81): Fe, 6.83; P, 0.82; W, 59.61; C, 6.79; N, 1.21. Found: Fe, 6.80; P, 0.84; W, 59.65; C, 6.82; N, 1.19. IR (KBr, cm^{-1}): 3406 (w), 1604 (s), 1407 (s), 1342 (m), 1072 (s), 962 (s), 887(s), 794 (s) (Figure S1).

4.3. Single-Crystal X-ray Crystallography. A good single crystal of **FeW−PYDC** with dimensions of 0.16 mm × 0.14 mm × 0.12 mm was prudently picked under an optical microscope and sealed in a glass tube closed at both ends. Intensity data were collected on a Bruker APEX-II CCD detector at 150 K with Mo Kα radiation (λ = 0.71073 Å). The structure was determined with olex2. The structure was determined using charge flipping and refined with the olex2 refinement package using Gauss−Newton minimization.[62,63]

Two paris of tungstate atoms (W2 and W2B or W6 and WB) have thermal parameters similar to the site occupancies of 70% and 30%. Two sites are located by N1/C5 and N2/C6 atoms in two pydc ligands with 50% occupancies due to the symmetrical feature. All H atoms on water molecules were directly included in the molecular formula. A summary of crystal data and structure refinements for compound **FeW−PYDC** is provided in Table 4.

4.4. Procedure for the Selective Oxidation of Alkanes. In a typical operation, alkanes (1 mmol), a powdered catalyst (0.3 mol %), a solvent (0.5 mL), and TBHP (70% aqueous solution, 3 mmol) were added successively to a tube at room temperature. The mixture was further placed on a parallel reactor and stirred for a certain time under preset conditions. The product was qualitatively detected by GC−MS, and the yield of the product was monitored by GC using naphthylene as the internal standard. At the end of each cycle, the catalyst was recovered by centrifugation after the reaction mixture was cooled to room temperature and then washed thoroughly (at least three times) with benzonitrile and dried in an oven at 100 °C overnight to be reused for the recyclability experiments.

■ ASSOCIATED CONTENT

Supporting Information

The Supporting Information is available free of charge at https://pubs.acs.org/doi/10.1021/acs.inorgchem.1c00135.

BVS, IR, selected bond lengths and angles, and additional catalytic properties of **FeW−PYDC** (PDF)

Accession Codes

CCDC 2015761 contains the supplementary crystallographic data for this paper. These data can be obtained free of charge via www.ccdc.cam.ac.uk/data_request/cif, or by emailing data_request@ccdc.cam.ac.uk, or by contacting The Cambridge Crystallographic Data Centre, 12 Union Road, Cambridge CB2 1EZ, UK; fax: +44 1223 336033.

■ AUTHOR INFORMATION

Corresponding Authors

Jingyang Niu − *Henan Key Laboratory of Polyoxometalate Chemistry, College of Chemistry and Chemical Engineering, Henan University, Kaifeng 475004, Henan, P. R. China;* orcid.org/0000-0001-6526-7767; Email: jyniu@henu.edu.cn

Jingping Wang − *Henan Key Laboratory of Polyoxometalate Chemistry, College of Chemistry and Chemical Engineering, Henan University, Kaifeng 475004, Henan, P. R. China;* Email: jpwang@henu.edu.cn

Authors

Quanzhong Wang − *Henan Key Laboratory of Polyoxometalate Chemistry, College of Chemistry and Chemical Engineering, Henan University, Kaifeng 475004, Henan, P. R. China*

Baijie Xu − *Henan Key Laboratory of Polyoxometalate Chemistry, College of Chemistry and Chemical Engineering, Henan University, Kaifeng 475004, Henan, P. R. China*

Yingyue Wang − *Henan Key Laboratory of Polyoxometalate Chemistry, College of Chemistry and Chemical Engineering, Henan University, Kaifeng 475004, Henan, P. R. China*

Hui Wang − *Henan Key Laboratory of Polyoxometalate Chemistry, College of Chemistry and Chemical Engineering, Henan University, Kaifeng 475004, Henan, P. R. China*

Xin Hu − *Henan Key Laboratory of Polyoxometalate Chemistry, College of Chemistry and Chemical Engineering, Henan University, Kaifeng 475004, Henan, P. R. China*

Pengtao Ma − *Henan Key Laboratory of Polyoxometalate Chemistry, College of Chemistry and Chemical Engineering, Henan University, Kaifeng 475004, Henan, P. R. China*

https://doi.org/10.1021/acs.inorgchem.1c00135
Inorg. Chem. 2021, 60, 7753−7761

Complete contact information is available at:
https://pubs.acs.org/10.1021/acs.inorgchem.1c00135

Notes

The authors declare no competing financial interest.

■ ACKNOWLEDGMENTS

The authors gratefully acknowledge the financial support from the National Natural Science Foundation of China (Grants 21571050, 21573056, 21771053, and 21771054).

■ REFERENCES

(1) Pham, P. H.; Doan, S. H.; Tran, H. T. T.; Nguyen, N. N.; Phan, A. N. Q.; Le, H. V.; Tu, T. N.; Phan, N. T. S. A New Transformation of Coumarins via Direct C−H Bond Activation Utilizing an Iron-Organic Framework as a Recyclable Catalyst. *Catal. Sci. Technol.* **2018**, *8*, 1267−1271.
(2) Moodie, L. W. K.; Chammaa, S.; Kindahl, T.; Hedberg, C. Palladium-Mediated Approach to Coumarin-Functionalized Amino Acids. *Org. Lett.* **2017**, *19*, 2797−2800.
(3) Daraie, M.; Lotfian, N.; Heravi, M. M.; Mirzaei, M. Chemoselective Synthesis of Drug-like Pyrrolo [2,3,4-Kl] Acridin-1-One Using Polyoxometalate@lanthanoid Catalyst. *React. Kinet., Mech. Catal.* **2020**, *129*, 391−401.
(4) Cao, L.; Zhao, Y.; Chu, Z.; Zhang, X.; Zhang, W. Core-Shell Magnetic Bimetallic MOF Material for Synergistic Enrichment of Phosphopeptides. *Talanta* **2020**, *206*, 120165.
(5) Zhang, Z.; Tao, Y.; Tian, H.; Yue, Q.; Liu, S.; Liu, Y.; Li, X.; Lu, Y.; Sun, Y.; Kraka, E.; Liu, S. Chelation-Assisted Selective Etching Construction of Hierarchical Polyoxometalate-Based Metal−Organic Framework. *Chem. Mater.* **2020**, *32*, 5550−5557.
(6) Zhao, X.; Gong, L.; Wang, C.; Wang, C.; Yu, K.; Zhou, B. A Facile Grinding Method for the Synthesis of 3D Ag Metal-Organic Frameworks (MOFs) Containing $Ag_6Mo_7O_{24}$ for High-Performance Supercapacitors. *Chem. - Eur. J.* **2020**, *26*, 4613−4619.
(7) Li, D.; Ma, P.; Niu, J.; Wang, J. Recent Advances in Transition-Metal-Containing Keggin-Type Polyoxometalate-Based Coordination Polymers. *Coord. Chem. Rev.* **2019**, *392*, 49−80.
(8) Li, D.; Ma, X.; Wang, Q.; Ma, P.; Niu, J.; Wang, J. Copper-Containing Polyoxometalate-Based Metal-Organic Frameworks as Highly Efficient Heterogeneous Catalysts toward Selective Oxidation of Alkylbenzenes. *Inorg. Chem.* **2019**, *58*, 15832−15840.
(9) Dun, R.; Wang, X.; Tan, M.; Huang, Z.; Huang, X.; Ding, W.; Lu, X. Quantitative Aerobic Oxidation of Primary Benzylic Alcohols to Aldehydes Catalyzed by Highly Efficient and Recyclable P_{123}-Stabilized Pd Nanoclusters in Acidic Aqueous Solution. *ACS Catal.* **2013**, *3*, 3063−3066.
(10) Xie, M.; Dai, X.; Meng, S.; Fu, X.; Chen, S. Selective oxidation of aromatic alcohols to corresponding aromatic aldehydes using In_2S_3 microsphere catalyst under visible light irradiation. *Chem. Eng. J.* **2014**, *245*, 107−116.
(11) Zhu, J.; Zhao, Y.; Tang, D.; Zhao, Z.; Carabineiro, S. A. Aerobic Selective Oxidation of Alcohols Using La1-xCexCoO$_3$ Perovskite Catalysts. *J. Catal.* **2016**, *340*, 41−48.
(12) Li, D.; Xu, Q.; Li, Y.; Qiu, Y.; Ma, P.; Niu, J.; Wang, J. A Stable Polyoxometalate-Based Metal-Organic Framework as Highly Efficient Heterogeneous Catalyst for Oxidation of Alcohols. *Inorg. Chem.* **2019**, *58*, 4945−4953.
(13) Wang, J.; Niu, J.; Zhang, M.; Ma, P.; Zhang, C.; Niu, J.; Wang, J. Organophosphonate-Functionalized Lanthanopolyoxomolybdate: Synthesis, Characterization, Magnetism, Luminescence, and Catalysis of H_2O_2-Based Thioether Oxidation. *Inorg. Chem.* **2018**, *57*, 1796−1805.
(14) Wang, K.; Niu, Y.; Zhao, D.; Zhao, Y.; Ma, P.; Zhang, D.; Wang, J.; Niu, J. The Polyoxovanadate-Based Carboxylate Derivative $K_6H[V^{V}_{17}V^{IV}_{12}(OH)_4O_{60}(OOC(CH_2)_4COO)_8]\cdot nH_2O$: Synthesis, Crystal Structure, and Catalysis for Oxidation of Sulfides. *Inorg. Chem.* **2017**, *56*, 14053−14059.
(15) Lu, J.; Ma, X.; Singh, V.; Zhang, Y.; Wang, P.; Feng, J.; Ma, P.; Niu, J.; Wang, J. Facile CO_2 Cycloaddition to Epoxides by Using a Tetracarbonyl Metal Selenotungstate Derivate $[\{Mn(CO)_3\}_4(Se_2W_{11}O_{43})]^{8-}$. *Inorg. Chem.* **2018**, *57*, 14632−14643.
(16) Tang, R.; Li, G.; Yu, J. Conformation-Induced Remote Meta-C−H Activation of Amines. *Nature* **2014**, *507*, 215−220.
(17) Liu, H.; Zhang, J.; Xu, X.; Wang, Q. A Polyoxometalate-Based Binder-Free Capacitive Deionization Electrode for Highly Efficient Sea Water Desalination. *Chem. - Eur. J.* **2020**, *26*, 4403−4409.
(18) Han, Q.; Qi, B.; Ren, W.; He, C.; Niu, J.; Duan, C. Polyoxometalate-Based Homochiral Metal-Organic Frameworks for Tandem Asymmetric Transformation of Cyclic Carbonates from Olefins. *Nat. Commun.* **2015**, *6*, 10007.
(19) Bryliakov, K. P.; Talsi, E. P. Active sites and mechanisms of bioinspired oxidation with H_2O_2, catalyzed by non-heme Fe and related Mn complexes. *Coord. Chem. Rev.* **2014**, *276*, 73−96.
(20) Groves, J. T. High-valent iron in chemical and biological oxidations. *J. Inorg. Biochem.* **2006**, *100*, 434−447.
(21) Nam, W. High-Valent Iron(IV)−Oxo Complexes of Heme and Non-Heme Ligands in Oxygenation Reactions. *Acc. Chem. Res.* **2007**, *40*, 522−531.
(22) Krebs, C.; Galonić Fujimori, D.; Walsh, C. T.; Bollinger, M., Jr. Non-Heme Fe(IV)−Oxo Intermediates. *Acc. Chem. Res.* **2007**, *40*, 484−492.
(23) McDonald, A. R.; Que, L., Jr. High-valent nonheme iron-oxo complexes: Synthesis, structure, and spectroscopy. *Coord. Chem. Rev.* **2013**, *257*, 414−428.
(24) Wolfe, M. D.; Lipscomb, J. D. Hydrogen Peroxide-coupled cis-Diol Formation Catalyzed by Naphthalene 1,2-Dioxygenase. *J. Biol. Chem.* **2003**, *278*, 829−835.
(25) Denisov, I. G.; Makris, T. M.; Sligar, S. G.; Schlichting, I. Structure and Chemistry of Cytochrome P450. *Chem. Rev.* **2005**, *105*, 2253−2278.
(26) Chen, Z.; Yin, G. The reactivity of the active metal oxo and hydroxo intermediates and their implications in oxidations. *Chem. Soc. Rev.* **2015**, *44*, 1083−1100.
(27) Zhang, Q.; Lei, D.; Luo, Q.; Wang, J.; Deng, T.; Zhang, Y.; Ma, P. Efficient Biodiesel Production from Oleic Acid Using Metal−Organic Framework Encapsulated Zr-Doped Polyoxometalate Nano-Hybrids. *RSC Adv.* **2020**, *10*, 8766−8772.
(28) Mukhopadhyay, S.; Basu, O.; Kar, A.; Das, S. K. Efficient Electrocatalytic Water Oxidation by Fe(Salen)-MOF Composite: Effect of Modified Microenvironment. *Inorg. Chem.* **2020**, *59*, 472−483.
(29) Jarrah, A.; Farhadi, S. Encapsulation of $K_6P_2W_{18}O_{62}$ into Magnetic Nanoporous Fe_3O_4/MIL-101(Fe) for Highly Enhanced Removal of Organic Dyes. *J. Solid State Chem.* **2020**, *285*, 121264.
(30) Wu, Y.; Liu, Y.; Huang, Y.; Xiao, G.; Li, Y.; Bai, Y.; Dang, D. Five Isomorphous Polyoxometalate-Based Inorganic-Organic Hybrid Materials Comprising 2D Metal-Organic Layers. *J. Solid State Chem.* **2020**, *286*, 121302.
(31) Yang, X.; Zhu, P.; Ma, X.; Li, W.; Tan, Z.; Sha, J. Graphite-like Polyoxometalate-Based Metal-Organic Framework as an Efficient Anode for Lithium Ion Batteries. *CrystEngComm* **2020**, *22*, 1340−1345.
(32) Sun, X.; Liu, S.; Zhang, S.; Dang, T.; Tian, H.; Lu, Y.; Liu, S. High Proton Conductivity Achieved by the Self-Assembly of POM-Based Acid-Base Adduct in SBA-15 over a Wide Range from −40 to 85 °C. *ACS Appl. Energy Mater.* **2020**, *3*, 1242−1248.
(33) Zhu, P.; Yang, X.; Li, X.; Sheng, N.; Zhang, H.; Zhang, G.; Sha, J. Insights into the Lithium Diffusion Process in a Defect-Containing Porous Crystalline POM@MOF Anode Material. *Dalton Trans* **2020**, *49*, 79−88.
(34) Han, Q.; He, C.; Zhao, M.; Qi, B.; Niu, J.; Duan, C. Engineering Chiral Polyoxometalate Hybrid Metal-Organic Frameworks for Asymmetric Dihydroxylation of Olefins. *J. Am. Chem. Soc.* **2013**, *135*, 10186−10189.
(35) He, J.; Li, J.; Han, Q.; Si, C.; Niu, G.; Li, M.; Wang, J.; Niu, J. Photoactive Metal-Organic Framework for the Reduction of Aryl

Halides by the Synergistic Effect of Consecutive Photo-Induced Electron-Transfer and Hydrogen-Atom Transfer Processes. *ACS Appl. Mater. Interfaces* **2020**, *12*, 2199−2206.
(36) He, J.; Han, Q.; Li, J.; Shi, Z.; Shi, X.; Niu, J. Ternary Supramolecular System for Photocatalytic Oxidation with Air by Consecutive Photo-induced Electron Transfer Processes. *J. Catal.* **2019**, *376*, 161−167.
(37) Shi, Z.; Li, J.; Han, Q.; Shi, Y.; Si, C.; Niu, G.; Ma, P.; Li, M. Polyoxometalate-Supported Aminocatalyst for the Photocatalytic Direct Synthesis of Imines from Alkenes and Amines. *Inorg. Chem.* **2019**, *58*, 12529−12533.
(38) Ishii, Y.; Yamawaki, K.; Ura, T.; Yamada, H.; Yoshida, T.; Ogawa, M. A Practical Method for Epoxidation of Terminal Olefins with 30% Hydrogen Peroxide under Halide-Free Conditions. *J. Org. Chem.* **1988**, *53*, 3587.
(39) Kumar, D.; Derat, E.; Khenkin, A.; Neumann, R.; Shaik, S. The high-valent iron-oxo species of polyoxometalate, if it can be made, will be a highly potent catalyst for C-H hydroxylation and double-bond epoxidation. *J. Am. Chem. Soc.* **2005**, *127*, 17712−17718.
(40) Zhang, Z.; Liu, Y.; Tian, H.; Li, X.; Liu, S.; Lu, Y.; Sun, Z.; Liu, T.; Liu, S. Polyoxometalate-Based Metal-Organic Framework Fractal Crystals. *Matter* **2020**, *2*, 250−260.
(41) Jia, W.; Zhang, J.; Lu, Z.; Wang, S.; Feng, S. Pt Decorated POMOF-Derived Constructions for Efficient Electrocatalytic Hydrogen Evolution. *Nanoscale* **2020**, *12*, 3902−3906.
(42) Buru, C. T.; Farha, O. K. Strategies for Incorporating Catalytically Active Polyoxometalates in Metal-Organic Frameworks for Organic Transformations. *ACS Appl. Mater. Interfaces* **2020**, *12*, 5345−5360.
(43) Li, J.; He, J.; Si, C.; Li, M.; Han, Q.; Wang, Z.; Zhao, J. Special-selective C−H oxidation of toluene to benzaldehyde by a hybrid polyoxometalate photocatalyst including a rare $[P_6W_{48}Fe_6O_{180}]^{30-}$ anion. *J. Catal.* **2020**, *392*, 244−253.
(44) Li, J.; Wang, X.; Song, G.; Lin, H.; Wang, X.; Liu, G. Various Anderson-Type Polyoxometalate-Based Metal-Organic Complexes Induced by Diverse Solvents: Assembly, Structures and Selective Adsorption for Organic Dyes. *Dalton Trans* **2020**, *49*, 1265−1275.
(45) Que, L., Jr.; Tolman, W. B. Biologically Inspired Oxidation Catalysis. *Nature* **2008**, *455* (8), 333−340.
(46) Ray, K.; Pfaff, F. F.; Wang, B.; Nam, W. Status of Reactive Non-Heme Metal-Oxygen Intermediates in Chemical and Enzymatic Reactions. *J. Am. Chem. Soc.* **2014**, *136*, 13942−13958.
(47) Armstrong, W. H.; Roth, M. E.; Lippard, S. J. Tetranuclear Iron-Oxo Complexes. Synthesis, Structure, and Properties of Species Containing the Nonplanar $\{Fe_4O_2\}^{8+}$ Core and Seven Bridging Carboxylate Ligands. *J. Am. Chem. Soc.* **1987**, *109*, 6318−6326.
(48) Gorun, S. M.; Lippard, S. J. Synthesis, Structure, and Characterization of the Tetranuclear Iron(III) Oxo Complex $[Fe_4O_2(BICOH)_2(BICO)_2(O_2CPh)_4]Cl_2$. *Inorg. Chem.* **1988**, *27*, 149−156.
(49) Grissom, T. G.; Plonka, A. M.; Sharp, C. H.; Ebrahim, A. M.; Tian, Y.; Collins-Wildman, D. L.; Kaledin, A. L.; Siegal, H. J.; Troya, D.; Hill, C. L.; Frenkel, A. I.; Musaev, D. G.; Gordon, W. O.; Karwacki, C. J.; Mitchell, M. B.; Morris, J. R. Metal-Organic Framework- and Polyoxometalate-Based Sorbents for the Uptake and Destruction of Chemical Warfare Agents. *ACS Appl. Mater. Interfaces* **2020**, *12*, 14641−14661.
(50) Zhou, K.; Shen, D.; Li, X.; Chen, Y.; Hou, L.; Zhang, Y.; Sha, J. Molybdenum Oxide-Based Metal-Organic Framework/Polypyrrole Nanocomposites for Enhancing Electrochemical Detection of Dopamine. *Talanta* **2020**, *209*, 120507.
(51) Huang, Q.; Liu, J.; Feng, L.; Wang, Q.; Guan, W.; Dong, L.; Zhang, L.; Yan, L.; Lan, Y.; Zhou, H. Multielectron Transportation of Polyoxometalate-Grafted Metalloporphyrin Coordination Frameworks for Selective CO_2-to-CH_4 Photoconversion. *Natl. Sci. Rev.* **2020**, *7*, 53−63.
(52) Brown, I. D.; Altermatt, D. Bond-Valence Parameters Obtained from a Systematic Analysis of the Inorganic Crystal Structure Database. *Acta Crystallogr., Sect. B: Struct. Sci.* **1985**, *41*, 244−247.
(53) Spek, A. Single-crystal structure validation with the program PLATON. *J. Appl. Crystallogr.* **2003**, *36*, 7−13.
(54) Shi, H.; Yan, G.; Zhang, Y.; Tan, H.; Zhou, W.; Ma, Y.; Li, Y.; Chen, W.; Wang, E. $Ag/AgxH_3-xPMO_{12}O_{40}$ nanowires with enhanced visible-light-driven photocatalytic performance. *ACS Appl. Mater. Interfaces* **2017**, *9*, 422−430.
(55) Chen, Y.; Huang, X.; Feng, X.; Li, J.; Huang, Y.; Zhao, J.; Guo, Y.; Dong, X.; Han, R.; Qi, P.; et al. Facile Fabrication of Magnetically Recyclable Metal−organic Framework Nanocomposites for Highly Efficient and Selective Catalytic Oxidation of Benzylic C−H Bonds. *Chem. Commun.* **2014**, *50*, 8374−8377.
(56) Hu, J.; Dong, J.; Huang, X.; Chi, Y.; Lin, Z.; Li, J.; Yang, S.; Ma, H.; Hu, C. Immobilization of Keggin Polyoxovanadoniobate in Crystalline Solids to Produce Effective Heterogeneous Catalysts towards Selective Oxidation of Benzyl-Alkanes. *Dalton Trans* **2017**, *46*, 8245−8251.
(57) Zou, C.; Zhang, Z.; Xu, X.; Gong, Q.; Li, J.; Wu, D. A Multifunctional Organic-Inorganic Hybrid Structure Based on Mn^{III}-Porphyrin and Polyoxometalate as a Highly Effective Dye Scavenger and Heterogenous Catalyst. *J. Am. Chem. Soc.* **2012**, *134*, 87−90.
(58) Hu, J.; Dong, J.; Huang, X.; Chi, Y.; Lin, Z.; Li, J.; Yang, S.; Ma, H.; Hu, C. Immobilization of Keggin Polyoxovanadoniobate in Crystalline Solids to Produce Effective Heterogeneous Catalysts towards Selective Oxidation of Benzyl-Alkanes. *Dalton Trans* **2017**, *46*, 8245−8251.
(59) Li, J.; Huang, X.; Yang, S.; Ma, H.; Chi, Y.; Hu, C. Four Alkoxohexavanadate-Based Pd-Polyoxovanadates as Robust Heterogeneous Catalysts for Oxidation of Benzyl-Alkanes. *Inorg. Chem.* **2015**, *54*, 1454−1461.
(60) Riemer, D.; Mandaviya, B.; Schilling, W.; Götz, A. C.; Kühl, T.; Finger, M.; Das, S. CO_2-Catalyzed Oxidation of Benzylic and Allylic Alcohols with DMSO. *ACS Catal.* **2018**, *8*, 3030−3034.
(61) Rocchiccioli-Deltcheff, C.; Fournier, M.; Franck, R.; Thouvenot, R. Vibrational Investigations of Polyoxometalates. 2. Evidence for Anion-Anion Interactions in Molybdenum(VI) and Tungsten(VI) Compounds Related to the Keggin Structure. *Inorg. Chem.* **1983**, *22*, 207−216.
(62) Dolomanov, O. V.; Bourhis, L. J.; Gildea, R. J.; Howard, J. A. K.; Puschmann, H. OLEX2: A Complete Structure Solu-tion, Refinement and Analysis Program. *J. Appl. Crystallogr.* **2009**, *42*, 339−341.
(63) Bourhis, L. J.; Dolomanov, O. V.; Gildea, R. J.; Howard, J. A. K.; Puschmann, H. The anatomy of a comprehensive constrained, restrained refinement program for the modern computing environment Olex2 dissected. *Acta Crystallogr., Sect. A: Found. Adv.* **2015**, *71*, 59−75.

https://doi.org/10.1021/acs.inorgchem.1c00135
Inorg. Chem. 2021, 60, 7753−7761